

## ORIGINAL ARTICLE

# Enhanced photoresponsivity of the MoS<sub>2</sub>-GaN heterojunction diode via the piezo-phototronic effect

Fei Xue<sup>1,2,3,5</sup>, Leijing Yang<sup>1,2,5</sup>, Mengxiao Chen<sup>1,2,3,5</sup>, Jian Chen<sup>1,2,3</sup>, Xiaonian Yang<sup>1,2,3</sup>, Longfei Wang<sup>1,2,3</sup>, Libo Chen<sup>1,2,3</sup>, Caofeng Pan<sup>1,2</sup> and Zhong Lin Wang<sup>1,2,4</sup>

Combining layered MoS<sub>2</sub> flakes with conventional 3D semiconductors is a feasible route to fabricate high-quality heterojunction devices by harnessing the advantages of both materials. Here, we present a pressure-modulated heterojunction photodiode that is composed of an *n*-type multilayer MoS<sub>2</sub> and a *p*-type GaN film via the piezo-phototronic effect. Under the illumination of 365 nm incident light, a strong photoresponse is observed with response and recovery times of ~66 and 74 ms, respectively. Under a pressure of 258 MPa, the photoresponsivity of this photodiode can be tuned by the piezo-phototronic effect arising from the GaN film to ~3.5 times. Because of the lowered junction barrier with an applied external pressure (strain), more photogenerated carriers can successfully pass through the junction area without recombination, which results in an enhancement effect. This work provides a possible path for the implementation of high-performance electronic and optoelectronic devices that are based on hybrid heterostructures via human interfacing.

NPG Asia Materials (2017) 9, e418; doi:10.1038/am.2017.142; published online 4 August 2017

## INTRODUCTION

Molybdenum disulfide (MoS<sub>2</sub>), a layered semiconductor from the family of transition metal dichalcogenides, has attracted considerable attention for the study of fundamental physics and high-performance nanodevices in ultrathin structures.<sup>1–4</sup> Semiconducting MoS<sub>2</sub> possesses a tunable bandgap that experiences transitions from a direct bandgap (~1.85 eV) in a monolayer to an indirect bandgap (~1.2 eV) in bulk films.<sup>1,5</sup> Atomically thin films of MoS<sub>2</sub> have been demonstrated as a unique channel material for field-effect transistors because of their high electron mobility, excellent current ON/OFF ratio and low subthreshold swing.<sup>3,4,6</sup> As an ideal photoactive semiconductor, MoS<sub>2</sub> flakes that are based on optoelectronic nanodevices have been successively developed for use in photovoltaics,<sup>7,8</sup> LEDs,<sup>9,10</sup> and photodetectors.<sup>11,12</sup>

The *p-n* heterojunction, in which two different types of doped semiconductors are sequentially stacked together, acts as fundamental building block for modern electronics and optoelectronics. To explore new observations and functionality, significant effort has been applied to construct ultrathin heterojunctions using MoS<sub>2</sub> flakes, including MoS<sub>2</sub>-WSe<sub>2</sub>,<sup>13,14</sup> MoS<sub>2</sub>-carbon nanotubes,<sup>15</sup> and MoS<sub>2</sub>-WS<sub>2</sub>.<sup>16,17</sup> In addition, combining layered MoS<sub>2</sub> flakes with conventional 3D semiconductors is also a feasible route to fabricate high-quality *p-n* heterojunctions by harnessing the advantages of both materials. For example, six-layered MoS<sub>2</sub> flakes and ZnO film-based *p-n* heterojunction diodes present a large forward-to-reverse current ratio ( $3.4 \times 10^4$ )

and a high external quantum efficiency (52.7%).<sup>18</sup> In addition, Si and monolayer MoS<sub>2</sub> based *p-n* diodes display strong exciton-dominant electroluminescence.<sup>19</sup> To date, regarding the progress of MoS<sub>2</sub>-GaN heterojunctions, Lee *et al.*<sup>20</sup> reported the excellent rectifying property of *p*-MoS<sub>2</sub> and *n*-GaN films; Ruzmetov *et al.*<sup>21</sup> showed the epitaxial growth of monolayer MoS<sub>2</sub> on a GaN film and demonstrated a *n<sup>+</sup>-n* heterojunction. However, a thorough study regarding the integration of exfoliated pristine *n*-type MoS<sub>2</sub> flakes and *p*-type GaN films for the application of photodetectors has not been conducted.

The piezo-phototronic effect utilizes piezoelectric polarization charges, which are induced at the surface of piezoelectric crystals by an applied strain, to tune/modulate the generation, separation and recombination of carriers in optoelectronic devices.<sup>22</sup> Remarkable performance improvements in solar cells,<sup>23,24</sup> LEDs,<sup>25,26</sup> and photodetectors<sup>27,28</sup> have been confirmed via the piezo-phototronic effect. As a traditional piezoelectric material, wurtzite GaN is intrinsically sensitive to an externally applied strain. The development of piezo-phototronic devices based on the GaN piezopotential, such as multilayer MoS<sub>2</sub> and GaN heterojunction devices, not only enhances performance of corresponding electronics but also contributes to the urgent demands of human interfacing.

Here, we present a vertically stacked heterojunction diode that consists of *n*-type multilayer MoS<sub>2</sub> and *p*-type GaN films. This device shows obvious rectification properties and the energy band diagrams

<sup>1</sup>Beijing Institute of Nanoenergy and Nanosystems, Chinese Academy of Sciences, Beijing, China; <sup>2</sup>CAS Center for Excellence in Nanoscience, National Center for Nanoscience and Technology (NCNST), Beijing, China; <sup>3</sup>University of Chinese Academy of Sciences, Beijing, China and <sup>4</sup>School of Material Science and Engineering, Georgia Institute of Technology, Atlanta, GA, USA

<sup>5</sup>These authors contributed equally to this work.

Correspondence: Professor ZL Wang or Professor C Pan, Beijing Institute of Nanoenergy and Nanosystems, Chinese Academy of Sciences, Tower-C, Techart Plaza, No. 30 Xueyuan Road, Haidian District, Beijing 100083, China.

E-mail: zhong.wang@mse.gatech.edu or Email: cfpan@binn.cas.cn

Received 24 April 2017; revised 31 May 2017; accepted 4 June 2017

of the classic *p-n* structure are proposed to illustrate the corresponding carrier transport process. Upon excitation with 365 nm light, the device exhibits a strong photoresponse with response and recovery times of ~66 and 74 ms, respectively. In addition, the applied strain dependence of the photocurrent for the heterojunction *p-n* diode is also demonstrated. Owing to the negative piezoelectric polarization charges that are induced at the top surface of the [0001]-oriented GaN film, the junction barrier of MoS<sub>2</sub> and GaN is lowered, so that more photogenerated carriers pass through the junction area and the related photoresponsivity is significantly increased by over a factor of 3.5.

## MATERIALS AND METHODS

### GaN film

The [0001]-oriented GaN films were synthesized on the *c*-plane polished sapphire substrate using a low-pressure MOCVD system. *p*-type GaN films with thicknesses of 4–5 μm are doped with Mg ions and the corresponding hole concentration is  $\sim 6 \times 10^{16} \text{ cm}^{-3}$ .

### Fabrication of the *p-n* heterojunction diode

The layered MoS<sub>2</sub> crystal was first exfoliated on a silicon substrate that was covered with 300 nm silica, which facilitated the identification and estimation of the crystal thickness using an optical microscope. In this work, due to the large production via the mechanical exfoliation method, samples with thicknesses of ~10–35 nm were chosen. Then, selected MoS<sub>2</sub> flakes were successfully transferred to the GaN film using the polymethyl methacrylate assisted wet chemical method, which formed the vertically stacked *p-n* heterojunction (bottom: GaN, top: MoS<sub>2</sub>). After patterning the heterojunction via UV exposure technology, a layer of insulator (60 nm Al<sub>2</sub>O<sub>3</sub>) was deposited via ALD, which separates the top electrode in contact with MoS<sub>2</sub> flakes and the bottom GaN semiconductor. E-beam evaporation was used to metallize the heterojunction devices and 5 nm Cr/50 nm Au was accurately deposited via the control system in the equipment. Finally, a layer of epoxy was employed

to package the photodiode, not only to protect the heterojunction from the damage of applied strain but also to maintain a uniform force on the junction area.

## RESULTS AND DISCUSSION

Figure 1a displays schematic and typical optical graphs of the as-fabricated heterojunction diode. As seen from Supplementary Figure S1, the thickness of MoS<sub>2</sub> flake in this device is ~23 nm. To characterize the *p-n* heterojunction, PL spectra of the *p*-GaN film are presented in Figure 1b. The gray line represents the fitting curve using Lorentzian functions. A strong PL emission peak, located at ~2.87 eV, is observed. As previously reported,<sup>1,5</sup> multilayer MoS<sub>2</sub> lacks a PL emission peak because of the indirect bandgap; therefore, the corresponding spectra is not shown here. Raman spectra of the heterojunction is also displayed in Figure 1c and Supplementary Figure S2. Two sharp peaks with high intensity at the left side of the image are assigned to in-plane E<sub>2g</sub> and out-plane A<sub>1g</sub> modes and the distance between those two photon vibrational modes is 25 cm<sup>-1</sup>, which agrees with the reported work for a bulk MoS<sub>2</sub> crystal.<sup>29</sup> A new Raman peak appears at 450 cm<sup>-1</sup>, which results from the stacked heterojunction. Because of the contribution of E<sub>2</sub> and A<sub>1</sub> longitudinal optical modes in the GaN film, two Raman peaks are also observed at 569 and 735 cm<sup>-1</sup>.<sup>30</sup>

To assess the device performance of the multilayer MoS<sub>2</sub> and GaN heterojunction diode, *I*–*V* measurements were performed and electric output properties are shown in Figure 2 and Supplementary Figure S3. A typical output characteristic of the heterojunction diode is indicated in Figure 2a. The contrastive experiments in Supplementary Figure S4 validate that the output current veritably comes from the *p-n* heterojunction. The inserted image presents the cross-sectional view and corresponding electrical connection of the device. The voltage bias is applied on the bottom electrode that contacts GaN film (anode) with the ground that is connected the top electrode (cathode). The output curve shows good rectification properties with a threshold voltage of 1 V, which allows the carrier transport to proceed at a forward bias, owing to a reduction in the junction potential barrier with a positive voltage bias. To clearly analyze the electric transport for the curve in Figure 2a, a semilogarithmic plot of the anode voltage dependence on the anode current is displayed in detail in Figure 2b. Because of the geometry of the atomically thin MoS<sub>2</sub>, a tunneling current is easily formed in the as-fabricated *p-n* heterojunction at a negative voltage bias.<sup>31</sup> Remarkably, the reverse tunneling current in the presented image is so large that it is comparable with the forward current. The correlated electric transport curve can be classified into four regions: (1) reverse tunneling region, (2) saturation current region, (3) ideal linear diode region, and (4) series-resistance-dominated region. In the case of region '1', at a low reverse bias, the electric-field-induced band bending is not severe and the direct tunneling (DT) modulates the carrier transport.<sup>31,32</sup> The relationship between the DT current and reverse bias is almost linear. In contrast, the junction barrier is further thinned by electric-field-induced band bending at a high reverse bias and Fowler–Nordheim tunneling (FNT) dominates the transport.<sup>31</sup> The relationship between the FNT and the reverse bias is nonlinear.

The energy band diagrams for interpreting the observed electric behaviors are schematically shown in Figure 2c. The work function and electron affinity values for multilayer MoS<sub>2</sub> and GaN films are  $\Phi_{\text{MoS}_2} = 5.4 \text{ eV}$ ,<sup>33</sup>  $\chi_{\text{MoS}_2} = 4 \text{ eV}$ <sup>34</sup> and  $\Phi_{\text{GaN}} = 7.5 \text{ eV}$ ,  $\chi_{\text{GaN}} = 4.1 \text{ eV}$ ,<sup>35</sup> respectively. Once those two semiconductors are stacked together, *n*-type multilayer MoS<sub>2</sub> will inherently deplete electrons at the junction area, which leads to upward band-bending; *p*-type GaN

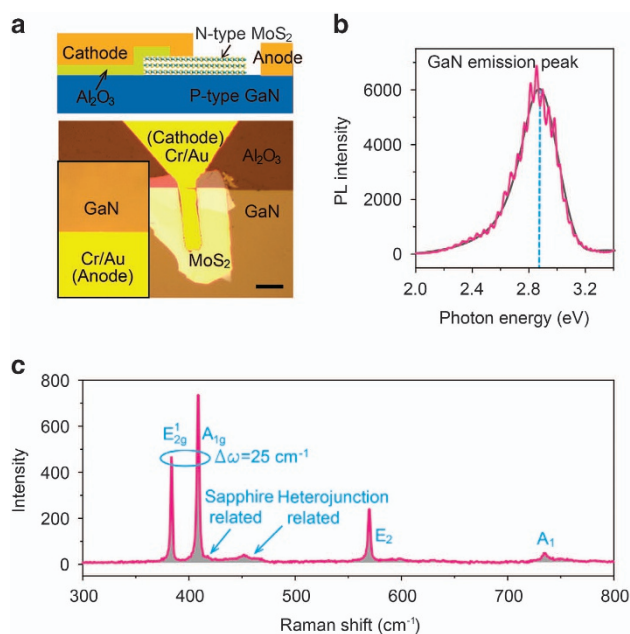


**Figure 1** Characterization of the GaN film and multilayer MoS<sub>2</sub> *p-n* heterojunction diode. (a) Illustration of the structure of the GaN and MoS<sub>2</sub> *p-n* diode and optical graphs of the device. The top electrode (cathode) is separated by a layer of insulator (Al<sub>2</sub>O<sub>3</sub>), and the bottom electrode (anode) that contacts the GaN film is inserted at the left side. The scale bar is 10 μm. (b) PL emission peak of the *p*-type GaN film. (c) Raman spectra of the GaN and MoS<sub>2</sub> *p-n* heterojunction. A new Raman peak appears at 450 cm<sup>-1</sup> that arises from the stacked heterojunction.

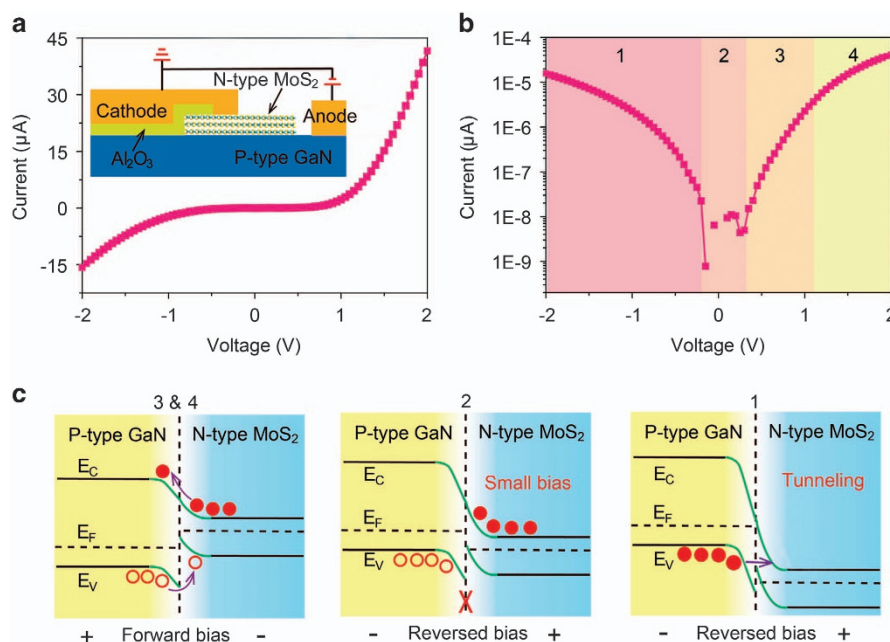


**Figure 2** Electric properties of the GaN film and multilayer MoS<sub>2</sub> *p-n* heterojunction diode. (a) Output characteristics for the *p-n* diode at room temperature. The top electrode (cathode) that is in contact with the multilayer MoS<sub>2</sub> is grounded and the bias applied on the other electrode is in contact with the GaN film. (b) Semi-logarithmic plot of the output curve that is shown in (a) to present the different carrier transport regions. (c) Energy band diagrams of the GaN and MoS<sub>2</sub> *p-n* heterojunction for interpreting the stated regions above. In region '1', the tunneling current dominates the carrier transport.

films deplete holes, which give rise to downward band-bending. Therefore, a junction barrier is formed for the *n*-MoS<sub>2</sub> and *p*-GaN heterojunction, as shown in Figure 2c. When the heterojunction undergoes a forward bias (regions '3' and '4'), the junction barrier is decreased; the Fermi-level of *n*-MoS<sub>2</sub> is raised and that of *p*-GaN is simultaneously lowered.<sup>32</sup> Moreover, a large amount of carriers will be injected into the junction (the left panel of Figure 2c) and the current that flows through the junction increases with an increase in the voltage bias. In region '2' (the saturation current region), when a small positive voltage bias is applied, the carriers cannot overcome the junction barrier to pass through the junction and the device maintains an off-state (the associated band diagram is similar with the left panel of Figure 2c and is not shown in the image); however, when a small negative voltage bias is applied, the depletion region is significantly enlarged, the junction barrier increases (the middle panel of Figure 2c), blocking carriers to pass through the junction. In the reverse tunneling region '1', a large reverse bias facilitates a thinning of the width of the junction barrier, which creates conditions that compel electrons to tunnel into the valence band of GaN films. With an increase in the reverse bias, the junction barrier width will be severely thinned and more electrons will tunnel through the heterojunction (the right panel of Figure 2c), which results in a large reversed current.

The photoperformance of the *p-n* heterojunction diode is also investigated and schematically displayed in Figure 3. In this work, ultraviolet light with a wavelength of 365 nm is used to excite the MoS<sub>2</sub> and GaN heterojunction device. As the power intensity of incident light gradually changes from 0 to 370 mW cm<sup>-2</sup>, the current drastically increases in the forward range (Figure 3a). Notably, under a small excited power density, the magnitude of the increase in current is more prominent. Because the photogenerated carriers in the photoactive semiconductors cannot effectively be separated by the inner electric field,<sup>36</sup> the increasing trend of current under a large power density of illumination is weakened. To present the photoresponse of the *p-n* heterojunction diode, the excited ultraviolet light is

controlled to periodically illuminate the devices with an irradiation time of 5 s. Under forward bias values of 0.5, 1 and 1.5 V, the histograms of the photoexcited current at various power densities are shown in Figure 3b. For comparison, the photocurrents ( $I_{ph} = I_{excited} - I_{dark}$ ), derived from the data in Figure 3b, are arranged and plotted as a function of power density (Figure 3d). Generally, the produced photocurrent for this photodetector is augmented by an increase in the voltage bias that was applied on the bottom electrode. Below a power density of 200 mW cm<sup>-2</sup>, the produced photocurrent rapidly increases as the power density increases and maintains a nearly linear relationship with the incident power density. While the excited power density exceeds 200 mW cm<sup>-2</sup>, the increase in photocurrent declines. Note that the changing trend in this excited range can be enlarged with an increase in the forward bias, especially above 1 V. This trend is mainly because excess photoexcited carriers can be separated due to the strong electric field that is applied to the heterojunction. To estimate the speed of the device photoresponse, a magnified current image is shown in Figure 3c. From the rising and falling edges of the photoexcited current, response and recovery times of 66 and 74 ms, respectively, are obtained for this heterojunction *p-n* diode, times that are approximately two orders of magnitude greater for photodetectors based on the structure of metal-MoS<sub>2</sub>-metal.<sup>12</sup>

With the rapid development of electronic skins, the development of electronic devices that can directly perceive external mechanical stimuli is urgently needed. In recent years, the newly emerging piezotronic and piezo-phototronic devices can use externally applied strain to tune electrical transport and directly convert strain to a change in semiconductor conductance via the piezo-electric polarization charges.<sup>25,26,37-40</sup> Next, we also demonstrated the piezo-phototronic-enhanced photocurrent for the as-fabricated MoS<sub>2</sub> and GaN heterojunction diode. Before illuminating the device, the output characteristics are depicted as a function of externally applied pressure (strain) in Figure 4a. A commercial digital dynamometer with a cylindrical probe of 5 mm in diameter is used to measure the applied

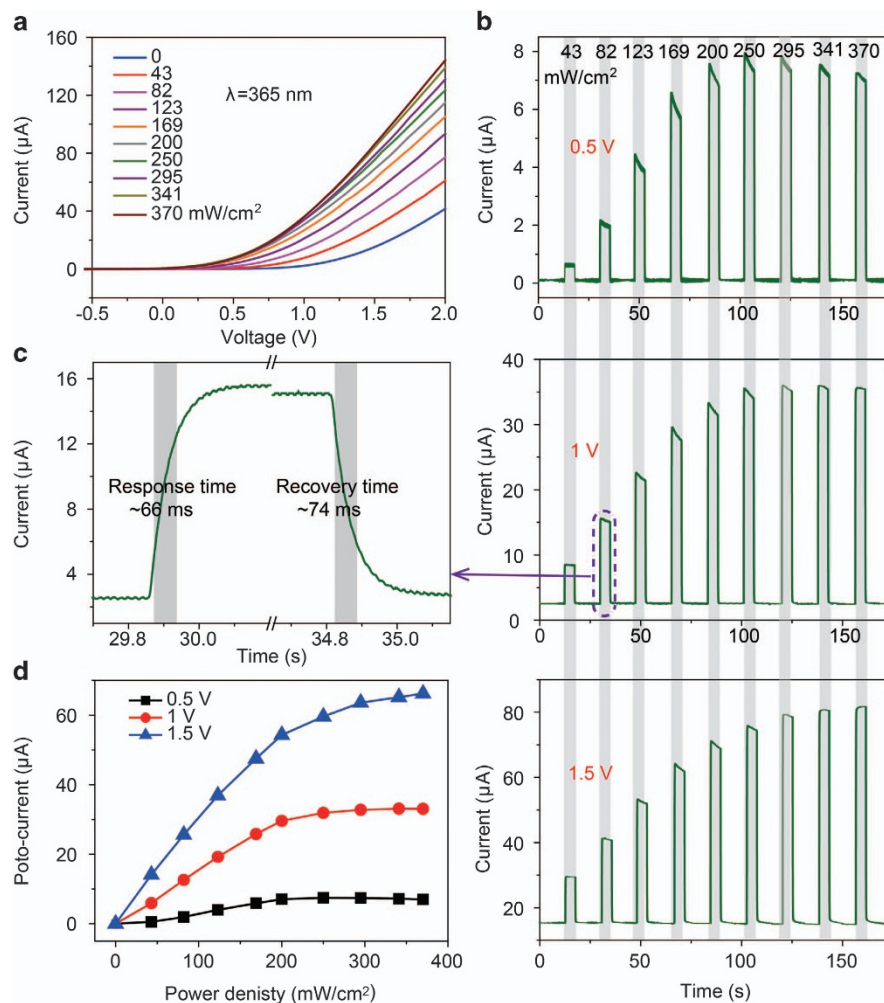


**Figure 3** Photoresponse of the GaN film and multilayer MoS<sub>2</sub> *p-n* heterojunction diode. (a) Output curves at various power densities of excited light for the *p-n* diode at room temperature. (b) Histogram of current responses at different power densities of excited light and various voltage bias conditions. The bias values applied to the *p-n* diode are successively 0.5, 1 and 1.5 V. (c) The enlarged current response image. The response and recovery times are  $\sim 66$  and 74 ms, respectively. (d) The power density dependence of the photocurrent with different voltage bias conditions.

pressure (strain) on the junction area. When a large pressure is applied, the relevant output current simultaneously increases, especially in a large forward bias, which is associated with the modulation of a junction barrier via piezoelectric charges (more details will be stated in the following paragraphs). Specifically, upon applying pressure, it is equivalent to imposing an extra positive voltage on the diode for an increased output current. Because of the pressure dependence of the output curves, the device can also be utilized as a functional strain sensor, as previously reported. Upon excitation at  $82 \text{ mW cm}^{-2}$ , the changes in the photocurrent under pressures of 123 and 258 MPa are shown in Figure 4b. With the illumination of incident light on the heterojunction device as a large pressure is applied, the corresponding photocurrent significantly increases. Note that a pressure of 258 MPa can enhance the photoresponsivity by  $\sim 3.5$  times (the inset image of Figure 4b), which strongly verifies that the strain-induced piezo-phototronic effect is an effective way to improve the photoperformance of devices.

Energy band diagrams are introduced to interpret the piezo-phototronic effect on the photoperformance of the *p-n* diode, as displayed in Figure 4c. Upon excitation with 365 nm light, the photoelectric effect occurs in both semiconducting materials (MoS<sub>2</sub>

and GaN) in this configuration and photo-excited electron-hole pairs are produced. Driven by the inner electric field, photo-generated electrons overcome the junction barrier to drift to the *p*-GaN side, whereas the photogenerated holes drift to the *n*-MoS<sub>2</sub> side (the left panel of Figure 4c),<sup>32</sup> which results in the observed photocurrent. Multilayer MoS<sub>2</sub> crystals (10–35 nm) lose the piezoelectric effect that exists in its monolayer, so the enhanced photocurrent with applied pressure (strain) is attributed to the piezopotential that is induced in the wurtzite GaN film. When a compressive strain is applied to the heterojunction, immobile and negative piezoelectric polarization charges will emerge at the top surface of the [0001]-oriented GaN film.<sup>41</sup> These negative piezoelectric charges attract positive holes from the GaN film (*p*-type) that aggregate in the depletion region via Coulomb forces and facilitate a decrease in the hole-depletion level, which gives rise to the decreased junction barrier (This is different from the modulation of negative piezoelectric charges in the barrier height for *n*-type ZnO semiconductors).<sup>41</sup> Therefore, motivated by the inner electric field of the forward bias, more carriers can pass through the heterojunction and the associated output current will be increased, as shown in Figure 4a. Similarly, for light illumination, more photogenerated carriers can drift through the lowered junction (the

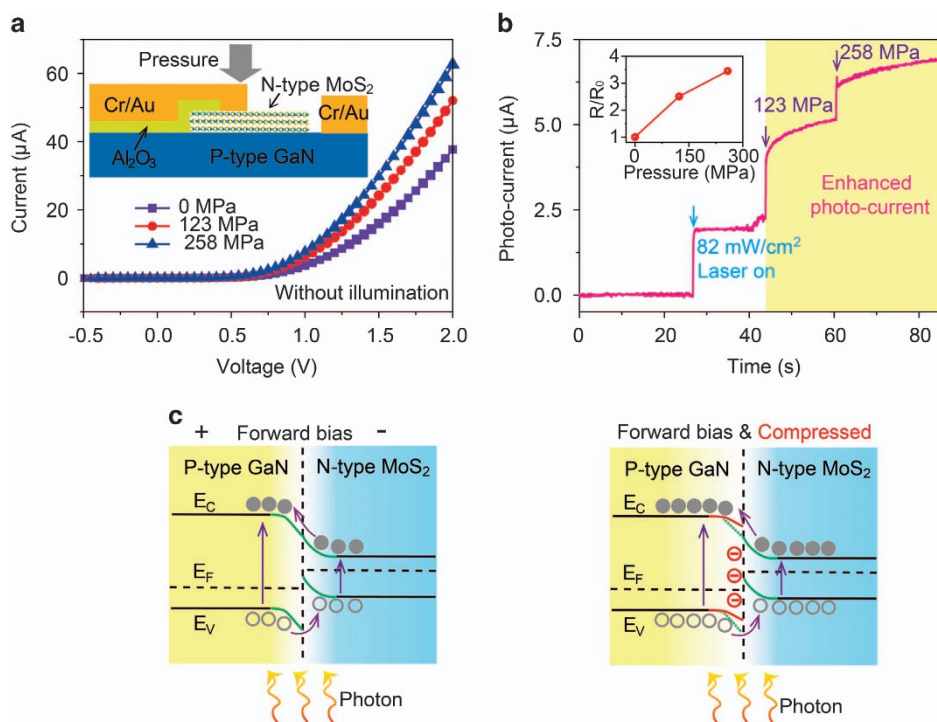


**Figure 4** Enhanced photoperformance of the GaN film and multilayer MoS<sub>2</sub> *p-n* heterojunction diode. (a) Output characteristics of the *p-n* diode under different compressive strains. With an increase in the applied strain, the current drastically increases. The inset presents a schematic of the testing set-up. (b) With incident light on the device, the photocurrent is enhanced by the pressure (strain). The inset shows the change in the relative photoresponsivity under different pressures. 'R' and 'R<sub>0</sub>' represent the actual photoresponsivity at different pressures and the photoresponsivity value without pressure, respectively. The voltage bias is fixed at 0.8 V. (c) Band diagrams to interpret the observed behaviors in (b). As the compressive strain is applied on the [0001]-oriented GaN film, negative piezoelectric charges are generated in the GaN film, which lowers the junction barrier and contributes to more photogenerated carriers passing through the junction. The gray circles and dots represent the photogenerated carriers.

right panel of Figure 4c) and macroscopically exhibit the increased photocurrent (or photoresponsivity) with applied pressure (strain), which is equivalent to increasing the voltage bias on the anode, as shown in Figure 3d.

## CONCLUSIONS

In conclusion, we have demonstrated a vertically stacked *p-n* heterojunction diode that is composed of a *p*-type GaN film and *n*-type multilayer MoS<sub>2</sub>. The electric output curve for the *p-n* diode exhibits clear rectification properties and energy band diagrams, which are based on the classic *p-n* structure, are proposed to interpret output characteristics. Under the irradiation of 365 nm light, the as-fabricated device shows excellent photoresponsivity with response and recovery times of 66 and 74 ms, respectively. Moreover, via the modulation of piezo-phototronic effect, the associated photoresponsivity for the *p-n* heterojunction diode is enhanced by ~3.5 times. This work provides a technical route to implement high-performance electronic and optoelectronic devices for human interfacing.

## CONFLICT OF INTEREST

The authors declare no conflict of interest.

## ACKNOWLEDGEMENTS

This research was supported by the 'thousands talents' program for a pioneer researcher and his innovation team, China, National Natural Science Foundation of China (Grant Nos 51432005, 5151101243, 51561145021).

## PUBLISHER'S NOTE

Springer Nature remains neutral with regard to jurisdictional claims in published maps and institutional affiliations.

- 1 Mak, K. F., Lee, C., Hone, J., Shan, J. & Heinz, T. F. Atomically thin MoS<sub>2</sub>: a new direct-gap semiconductor. *Phys. Rev. Lett.* **105**, 136805 (2010).
- 2 Mak, K. F., He, K., Lee, C., Lee, G. H., Hone, J., Heinz, T. F. & Shan, J. Tightly bound trions in monolayer MoS<sub>2</sub>. *Nat. Mater.* **12**, 207–211 (2013).
- 3 Radisavljevic, B., Radenovic, A., Brivio, J., Giacometti, V. & Kis, A. Single-layer MoS<sub>2</sub> transistors. *Nat. Nanotechnol.* **6**, 147–150 (2011).
- 4 Kim, S., Konar, A., Hwang, W. S., Lee, J. H., Lee, J., Yang, J., Jung, C., Kim, H., Yoo, J. B., Choi, J. Y., Jin, Y. W., Lee, S. Y., Jena, D., Choi, W. & Kim, K. High-mobility and low-power thin-film transistors based on multilayer MoS<sub>2</sub> crystals. *Nat. Commun.* **3**, 1011 (2012).
- 5 Ganatra, R. & Zhang, Q. Few-layer MoS<sub>2</sub>: a promising layered semiconductor. *ACS Nano* **8**, 4074–4099 (2014).
- 6 Cheng, R., Jiang, S., Chen, Y., Liu, Y., Weiss, N., Cheng, H. C., Wu, H., Huang, Y. & Duan, X. F. Few-layer molybdenum disulfide transistors and circuits for high-speed flexible electronics. *Nat. Commun.* **5**, 5143 (2014).
- 7 Fontana, M., Deppe, T., Boyd, A. K., Rinzan, M., Liu, A. Y., Paranjape, M. & Barbara, P. Electron-hole transport and photovoltaic effect in gated MoS<sub>2</sub> Schottky junctions. *Sci. Rep.* **3**, 1634 (2013).
- 8 Wi, S., Kim, H., Chen, M. K., Nam, H., Guo, L. J., Meyhofer, E. & Liang, X. G. Enhancement of photovoltaic response in multilayer MoS<sub>2</sub> induced by plasma doping. *ACS Nano* **8**, 5270–5281 (2014).
- 9 Cheng, R., Li, D. H., Zhou, H. L., Wang, C., Yin, A. X., Jiang, S., Liu, Y., Chen, Y., Huang, Y. & Duan, X. F. Electroluminescence and photocurrent generation from atomically sharp WSe<sub>2</sub>/MoS<sub>2</sub> heterojunction *p-n* diodes. *Nano Lett.* **14**, 5590–5597 (2014).
- 10 Sundaram, R. S., Engel, M., Lombardo, A., Krupke, R., Ferrari, A. C., Avouris, P. & Steiner, M. Electroluminescence in single layer MoS<sub>2</sub>. *Nano Lett.* **13**, 1416–1421 (2013).
- 11 Choi, W., Cho, M. Y., Konar, A., Lee, J. H., Cha, G. B., Hong, S. C., Kim, S., Kim, J., Jena, D., Joo, J. & Kim, S. High-detectivity multilayer MoS<sub>2</sub> phototransistors

- with spectral response from ultraviolet to infrared. *Adv. Mater.* **24**, 5832–5836 (2012).
- 12 Lopez-Sanchez, O., Lembke, D., Kayci, M., Radenovic, A. & Kis, A. Ultrasensitive photodetectors based on monolayer MoS<sub>2</sub>. *Nat. Nanotechnol.* **8**, 497–501 (2013).
  - 13 Li, M. Y., Shi, Y. M., Cheng, C. C., Lu, L. S., Lin, Y. C., Tang, H. L., Tsai, M.-L., Chu, C.-W., Wei, K.-H., He, J.-H., Chang, W.-H., Suenaga, K. & Li, L.-J. Epitaxial growth of a monolayer WSe<sub>2</sub>-MoS<sub>2</sub> lateral p-n junction with an atomically sharp interface. *Science* **349**, 524–528 (2015).
  - 14 Chiu, M. H., Zhang, C. D., Shiu, H. W., Chuu, C. P., Chen, C. H., Chang, C. Y. S., Chen, C.-H., Chou, M.-Y., Shih, C.-K. & Li, L.-J. Determination of band alignment in the single-layer MoS<sub>2</sub>/WSe<sub>2</sub> heterojunction. *Nat. Commun.* **6**, 7666 (2015).
  - 15 Jariwala, D., Sangwan, V. K., Wu, C. C., Prabhuramirashi, P. L., Geier, M. L., Marks, T. J., Lincoln, J. L. & Hersam, M. C. Gate-tunable carbon nanotube-MoS<sub>2</sub> heterojunction p-n diode. *Proc. Natl Acad. Sci. USA* **110**, 18076–18080 (2013).
  - 16 Hong, X. P., Kim, J., Shi, S. F., Zhang, Y., Jin, C. H., Sun, Y. H., Tongay, S., Wu, J., Zhang, Y. & Wang, F. Ultrafast charge transfer in atomically thin MoS<sub>2</sub>/WS<sub>2</sub> heterostructures. *Nat. Nanotechnol.* **9**, 682–686 (2014).
  - 17 Huo, N. J., Kang, J., Wei, Z. M., Li, S. S., Li, J. B. & Wei, S. H. Novel and enhanced optoelectronic performances of multilayer MoS<sub>2</sub>-WS<sub>2</sub> heterostructure transistors. *Adv. Funct. Mater.* **24**, 7025–7031 (2014).
  - 18 Xue, F., Chen, L. B., Chen, J., Liu, J. B., Wang, L. F., Chen, M. X., Pang, Y. K., Yang, X. N., Gao, G. Y., Zhai, J. Y. & Wang, Z. L. p-Type MoS<sub>2</sub> and n-Type ZnO diode and its performance enhancement by the piezophototronic effect. *Adv. Mater.* **28**, 3391–3398 (2016).
  - 19 Ye, Y., Ye, Z., Gharghi, M., Zhu, H., Zhao, M., Wang, Y., Yin, X. & Zhang, X. Exciton-dominant electroluminescence from a diode of monolayer MoS<sub>2</sub>. *Appl. Phys. Lett.* **104**, 193508 (2014).
  - 20 Lee, E. W., Lee, C. H., Paul, P. K., Ma, L., McCulloch, W. D., Krishnamoorthy, S., Wu, Y. Y., Arehart, A. R. & Rajan, S. Layer-transferred MoS<sub>2</sub>/GaN PN diodes. *Appl. Phys. Lett.* **107**, 103505 (2015).
  - 21 Ruzmetov, D., Zhang, K., Stan, G., Kalanyan, B., Bhimanapati, G. R., Eichfeld, S. M., Bruke, R. A., Shah, P. B., O'Regan, T. P., Crowne, F. J., Birdwell, A. G., Robinson, J. A., Davydov, A. V. & Ivanov, T. G. Vertical 2D/3D semiconductor heterostructures based on epitaxial molybdenum disulfide and gallium nitride. *ACS Nano* **10**, 3580–3588 (2016).
  - 22 Pan, C. F., Dong, L., Zhu, G., Niu, S. M., Yu, R. M., Yang, Q., Liu, Y. & Wang, Z. L. High-resolution electroluminescent imaging of pressure distribution using a piezo-electric nanowire LED array. *Nat. Photonics* **7**, 752–758 (2013).
  - 23 Zhu, L., Wang, L., Pan, C., Chen, L., Xue, F., Chen, B., Yang, L., Su, L. & Wang, Z. L. Enhancing the efficiency of silicon-based solar cells by the piezo-phototronic effect. *ACS Nano* **11**, 1894–1900 (2017).
  - 24 Zhu, L. P., Wang, L. F., Xue, F., Chen, L. B., Fu, J. Q., Feng, X. L., Li, T. & Wang, Z. L. Piezo-phototronic effect enhanced flexible solar cells based on n-ZnO/p-SnS core-shell nanowire array. *Adv. Sci.* **4**, 1600185 (2017).
  - 25 Li, X., Chen, M., Yu, R., Zhang, T., Song, D., Liang, R., Zhang, Q., Cheng, S., Dong, L., Pan, A., Wang, Z. L., Zhu, J. & Pan, C. Enhancing light emission of ZnO-nanofilm/Si-micropillar heterostructure arrays by piezo-phototronic effect. *Adv. Mater.* **27**, 4447–4453 (2015).
  - 26 Chen, M., Pan, C., Zhang, T., Li, X., Liang, R. & Wang, Z. L. Tuning light emission of a pressure-sensitive silicon/ZnO nanowires heterostructure matrix through piezo-phototronic effects. *ACS Nano* **10**, 6074–6079 (2016).
  - 27 Zhang, Z., Liao, Q. L., Yu, Y. H., Wang, X. D. & Zhang, Y. Enhanced photoresponse of ZnO nanorods-based self-powered photodetector by piezotronic interface engineering. *Nano Energy* **9**, 237 (2014).
  - 28 Han, X., Du, W. M., Yu, R. M., Pan, C. F. & Wang, Z. L. Piezo-phototronic enhanced UV sensing based on a nanowire photodetector array. *Adv. Mater.* **27**, 7963–7969 (2015).
  - 29 Li, H., Zhang, Q., Yap, C. C. R., Tay, B. K., Edwin, T. H. T., Olivier, A. & Baillargeat, D. From bulk to monolayer MoS<sub>2</sub>: evolution of raman scattering. *Adv. Funct. Mater.* **22**, 1385–1390 (2012).
  - 30 Limmer, W., Ritter, W., Sauer, R., Mensching, B., Liu, C. & Rauschenbach, B. Raman scattering in ion-implanted GaN. *Appl. Phys. Lett.* **72**, 2589 (1998).
  - 31 Li, H. M., Lee, D., Qu, D., Liu, X., Ryu, J., Seabaugh, A. & Yoo, W. J. Ultimate thin vertical p-n junction composed of two-dimensional layered molybdenum disulfide. *Nat. Commun.* **6**, 6564 (2015).
  - 32 Size, S. M. & Ng, K. K. *Physics of Semiconductor Devices*, (John Wiley & Sons, 1981).
  - 33 Kim, J. H., Lee, J., Kim, J. H., Hwang, C. C., Lee, C. & Park, J. Y. Work function variation of MoS<sub>2</sub> atomic layers grown with chemical vapor deposition: the effects of thickness and the adsorption of water/oxygen molecules. *Appl. Phys. Lett.* **106** (2015).
  - 34 Chen, C., Qiao, H., Lin, S., Man, Luk, C., Liu, Y., Xu, Z., Song, J., Xue, Y., Li, D., Yuan, J., Yu, W., Pan, C., Lau, S. P. & Bao, Q. L. Highly responsive MoS<sub>2</sub> photodetectors enhanced by graphene quantum dots. *Sci. Rep.* **5**, 11830 (2015).
  - 35 Jeong, H., Bang, S., Oh, H. M., Jeong, H. J., An, S. J., Han, G. H., Kim, H., Kim, K. K., Park, J. C., Lee, Y. H., Leronde, G. & Jeong, M. S. Semiconductor-insulator-semiconductor diode consisting of monolayer MoS<sub>2</sub>, h-BN, and GaN heterostructure. *ACS Nano* **9**, 10032–10038 (2015).
  - 36 Peng, M. Z., Liu, Y. D., Yu, A. F., Zhang, Y., Liu, C. H., Liu, J. Y., Wu, W., Zhang, K., Shi, X., Kou, J., Zhai, J. & Wang, Z. L. Flexible self-powered GaN ultraviolet photoswitch with piezo-phototronic effect enhanced on/off ratio. *ACS Nano* **10**, 1572–1579 (2016).
  - 37 Xue, F., Zhang, L. M., Tang, W., Zhang, C., Du, W. M. & Wang, Z. L. Piezotronic effect on ZnO nanowire film based temperature sensor. *ACS Appl. Mater. Inter.* **6**, 5955–5961 (2014).
  - 38 Xue, F., Zhang, L. M., Feng, X. L., Hu, G. F., Fan, F. R., Wen, X. N., Zheng, L. & Wang, Z. L. Influence of external electric field on piezotronic effect in ZnO nanowires. *Nano Res.* **8**, 2390 (2015).
  - 39 Chen, L. B., Xue, F., Li, X. H., Huang, X., Wang, L. F., Kou, J. Z. & Wang, Z. L. Strain-Gated field effect transistor of a MoS<sub>2</sub> ZnO 2D-1D hybrid structure. *ACS Nano* **10**, 1546–1551 (2016).
  - 40 Wu, W., Wang, L., Li, Y., Zhang, F., Lin, L., Niu, S., Chenet, D., Zhang, X., Hao, Y., Heinz, T. F., Hone, J. & Wang, Z. L. Piezoelectricity of single-atomic-layer MoS<sub>2</sub> for energy conversion and piezotronics. *Nature* **514**, 470–474 (2014).
  - 41 Hu, Y., Zhang, Y., Lin, L., Ding, Y., Zhu, G. & Wang, Z. L. Piezo-phototronic effect on electroluminescence properties of p-type GaN thin films. *Nano Lett.* **12**, 3851–3856 (2012).



This work is licensed under a Creative Commons Attribution 4.0 International License. The images or other third party material in this article are included in the article's Creative Commons license, unless indicated otherwise in the credit line; if the material is not included under the Creative Commons license, users will need to obtain permission from the license holder to reproduce the material. To view a copy of this license, visit <http://creativecommons.org/licenses/by/4.0/>

© The Author(s) 2017

Supplementary Information accompanies the paper on the NPG Asia Materials website (<http://www.nature.com/am>)